Study of IPMSM Interturn Faults Part I: Development and Analysis of Models With Series and Parallel Winding Connections

Bon-Gwan Gu

***Abstract*—In this study, the interturn fault (ITF) models of interior permanent magnet synchronous motors (IPMSMs) employing series and parallel winding connections were developed through the addition of saliency modeling to the surface-mounted permanent magnet motor models presented in a previous work. The saliency model was obtained by using deformed flux models based on both the fault winding flux information and inductance variations caused by cross-flux linkages that depend on the distribution of same-phase windings. By assuming a balanced three-phase current injection, positive and negative sequence voltages, and the fault current are obtained in the positive and negative synchronous reference frames. The output torque models were developed by adding the magnet and reluctance torques, which were derived from the developed models. To verify the proposed IPMSM models with an ITF, a finite element method-based simulation and experimental measurements were performed; the results are presented in this paper.**

***Index Terms*—Interturn fault, IPMSM, negative sequence, positive sequence.**

I. Introduction

OWING to their high efficiency and power density, the permanent magnet synchronous motors (PMSMs) are favored for many applications such as industrial drives, home appliances, and electric vehicles (EVs) [1]–[3]. PMSM can be categorized as surface PMSMs (SPMSMs) or interior PMSMs (IPMSMs) depending on the permanent magnet position. The IPMSM has a more complicated electrical model than the SPMSM based on the saliency. However, because of the saliency, the IPMSM has high torque and power densities.

An IPMSM normally works as the main motive power source for mechanical movement in many applications. Hence, the motor fault detection function of the motor drive is a major reliability index for the whole system. For example, the EV traction motor fault is a severe problem because it directly disables the vehicle propulsion function. However, if a fault is detected and the driver is informed early enough that the traction motor can propel the vehicle to a nearby repair shop, the unwanted vehicle stoppages can be avoided.

Manuscript received May 24, 2015; revised August 9, 2015; accepted September 17, 2015. Date of publication October 29, 2015; date of current version March 2, 2016. This work was supported by the National Research Foundation of Korea (NRF) Grant funded by the Korea Government (MSIP) (2015R1C1A1A01052647). Recommended for publication by Associate Editor F. Khan.

The author is with the School of Energy Engineering, Kyungpook National University, Daegu 702-701, Korea (e-mail: bggu@knu.ac.kr).

Color versions of one or more of the figures in this paper are available online at http://ieeexplore.ieee.org.

Digital Object Identifier 10.1109/TPEL.2015.2496142

A common motor fault is the winding turn short, which is caused by coil insulation failure [4]–[6], [8], [9], [11], [14], [20], [23]. As the coil insulation material is under high voltage and temperature stresses, it gradually deteriorates and finally loses its insulating characteristics; this is called an interturn fault (ITF). When this happens, the shorted turns configure an extra circuit loop coupled to flux linkages by other motor windings and the rotor magnet. Owing to the low impedance and high-coupled flux linkage voltage, a high-fault current is thus induced in the ITF windings, which generates ohmic loss and heat that further weaken the surrounding insulation material [7]. Through this process of positive feedback, an ITF can easily expand into nearby windings, enlarging a small ITF into a severe one [26]. The large fault current in the additional current path can also produce irreversible demagnetization of the rotor permanent magnets [22], [27]. Therefore, it is essential to detect and manage incipient ITFs.

If an ITF occurs, there are imbalances in the three-phase impedance and back-electromotive force (EMF); as a result, negative sequence terms are induced within the motor current or voltage. A number of previous studies have used imbalanced data to detect ITFs [9]–[14] and unexpected frequency currents or voltages [15], [16]. Although these fault detection schemes are simple and easy to implement, they require the fault threshold level to be predefined based on rich motor pretest data owing to the absence of accurate PMSM models subjected to an ITF. If accurate ITF models of the PMSM can be derived, the pretest to define the threshold level will be much simpler. Hence, to implement an ITF detection method for a specific motor, deriving an adequate IPMSM model that incorporates an ITF is required. A number of previous studies have developed SPMSM models. Other studies [17]–[24] have produced ITF models of PMSMs by using the winding function [17], [22] or a simplified model [18]–[21], [23], [24] to derive the motor inductance arising from ITFs. However, such models are inaccurate with respect to multipole motors because they ignore flux couplings between ITF windings and healthy windings in the same phase. Romeral *et al.* [21] and Jeong *et al.* [24] proposed simplified fault models. Their inductance models assume that the ITF happens equally on every winding set of the motor in proportion to the turn short fault ratio. However, an ITF normally occurs in one winding set. Hence, the ITF induces a flux unbalance in the motor. Gu *et al.* [25] modeled this kind of problem. However, such models are inaccurate with respect to multipole motors because they ignore flux couplings between turn-faulted winding and other healthy windings in the same phase.

Gu *et al.* [26] developed ITF models of SPMSMs employing series and parallel winding connections by using deformed flux models based on both the fault winding flux information and the inductance variations caused by cross-flux linkages that depend on the distribution of the same phase windings. IPMSMs are similar to SPMSMs except for the magnetic saliency. The saliency induces an inductance variation depending on the rotor position, which makes the IPMSM model more complicated. In this study, a direct quadrate (*d*-*q*) model of an IPMSM experiencing an ITF was developed in the positive and the negative sequence synchronous reference frames (SRFs). Both series and parallel winding IPMSMs were modeled by adding the saliency effect to the SPMSM model. First, a fault current conducting a fault winding was derived. Then, the *d*-*q* positive and negative sequence voltages from only the saliency were derived and added to the SPMSM model for the complete IPMSM model with an ITF. A finite element method (FEM) simulation and back-EMF measurement were conducted to validate the proposed model.

II. IPMSM Model With Series-Connected Winding

Fig. 1 shows the (a) six-pole nine-slot IPMSM with concentric windings and (b) winding configuration of a series connection subjected to an ITF. Here, $a1$, $a2$, $a3$, $b1$, $b2$, $b3$, $c1$, $c2$, and $c3$ are the winding numbers of each phase; i_a, i_b, and i_c, denote the phase currents; v_a, v_b, and v_c denote the voltages of the a-, b-, and c-phase windings. As insulation failures do not provide a zero resistance path, as discussed by Jeong *et al.* [24] and Gu *et al.* [26], the failure spot can be described as the fault resistance R_f with the ITF current i_f. The a-phase winding is assumed to have an ITF. The turn short fault winding shown in Fig. 1 makes another fault circuit loop composed of the fault resistance R_f, a fault winding inductance, and a fault winding flux linkage.

Because of the rotor saliency, the self- and cross-coupling inductances of the healthy IPMSM vary depending on the electrical rotor angle θ: see (1) shown at the bottom of the next page. where $L_1 = \frac{L_d + L_q}{3}$ and $L_2 = \frac{L_q - L_d}{3}$. L_d, L_q, and L_l denote the *d*- and *q*-axis stator inductances in the SRF and the leakage inductance. L_2 represents the saliency inductance. If L_2 is zero ($L_d = L_q$), the saliency effect vanishes, and the inductance model (1) is equal to that of the SPMSM. Although the self- and cross-inductances contain sine and cosine terms, they are summed to be constant values when the IPMSM dynamic equation is transformed into the SRF. That simplifies the dynamic IPMSM model in the SRF enough for it to be utilized in the motor drive design and analysis. However, an IPMSM with an ITF has a more complicated inductance matrix because of the fault winding interference with the balanced flux linkages.

The IPMSM magnetic coupling path between each phase winding is the same as that of the SPMSM except for saliency; the inductance variation by the ITF can be described as that of the SPMSM excluding the saliency. Here, the healthy turn ratio of $a1$ is defined as $x = N_{\text{healthy}}/N$, where N_{healthy} and N denote the $a1$ winding healthy turn number and total turn number. Hence, for an SPMSM model with an ITF [26] and (1), the IPMSM voltage equation can be derived as follows:

$$\begin{bmatrix} v_a \\ v_b \\ v_c \\ 0 \end{bmatrix} = \mathbf{R_s} \begin{bmatrix} i_a \\ i_b \\ i_c \\ i_f \end{bmatrix} + \frac{d}{dt}\mathbf{L_s} \begin{bmatrix} i_a \\ i_b \\ i_c \\ i_f \end{bmatrix} + \omega\psi_m \begin{bmatrix} -(1-(1-x)2/P)\sin\theta \\ -\sin(\theta - 2\pi/3) \\ -\sin(\theta + 2\pi/3) \\ -(1-x)(2/P)\sin\theta \end{bmatrix} \quad (2)$$

where

$$\mathbf{R_s} = \begin{bmatrix} R_{s11} & 0 & 0 & R_{s14} \\ 0 & R_{s22} & 0 & 0 \\ 0 & 0 & R_{s33} & 0 \\ R_{s41} & 0 & 0 & R_{s44} \end{bmatrix},$$

$$\mathbf{L_s} = \begin{bmatrix} L_{s11} & L_{s12} & L_{s13} & L_{s14} \\ L_{s21} & L_{s22} & L_{s23} & L_{s24} \\ L_{s31} & L_{s32} & L_{s33} & L_{s34} \\ L_{s41} & L_{s42} & L_{s43} & L_{s44} \end{bmatrix}$$

$$R_{s11} = R + (x-1)\frac{2}{P}R + R_f, R_{s14} = R_{s41} = -R_f,$$

$$R_{s22} = R_{s33} = R, R_{s44} = (1-x)\frac{2}{P}R + R_f$$

$$L_{sij} = \begin{cases} k_{sij}(L_1 - L_2\cos 2\theta) & \text{if (i,j)} = (1,1), \\ & (1,4),(4,1),(4,4) \\ k_{sij}\left(L_1 - L_2\cos(2\theta + \frac{2\pi}{3})\right) & \text{if (i,j)} = (2,2) \\ k_{sij}\left(L_1 - L_2\cos(2\theta - \frac{2\pi}{3})\right) & \text{if (i,j)} = (3,3) \\ k_{sij}(L_1 + 2L_2\cos 2\theta) & \text{if (i,j)} = (2,3), \\ & (3,2) \\ k_{sij}\left(L_1 + 2L_2\cos(2\theta - \frac{2\pi}{3})\right) & \text{if (i,j)} = (1,2), \\ & (2,1),(2,4),(4,2) \\ k_{sij}\left(L_1 + 2L_2\cos(2\theta + \frac{2\pi}{3})\right) & \text{if (i,j)} = (1,3), \\ & (3,1),(3,4),(4,3) \end{cases}$$

$$k_{s11} = 1 + \frac{2(x^2-1)}{P(1-\gamma)} + \frac{4\gamma(1-x)}{P(1-\gamma)}, \quad k_{s12} = k_{s21} = k_{s13} = k_{s31} = -\frac{1}{2} + \frac{1-x}{P}$$

$$k_{s22} = k_{s33} = 1, k_{s23} = k_{s32} = -\frac{1}{2}, \quad k_{s14} = k_{s41}$$

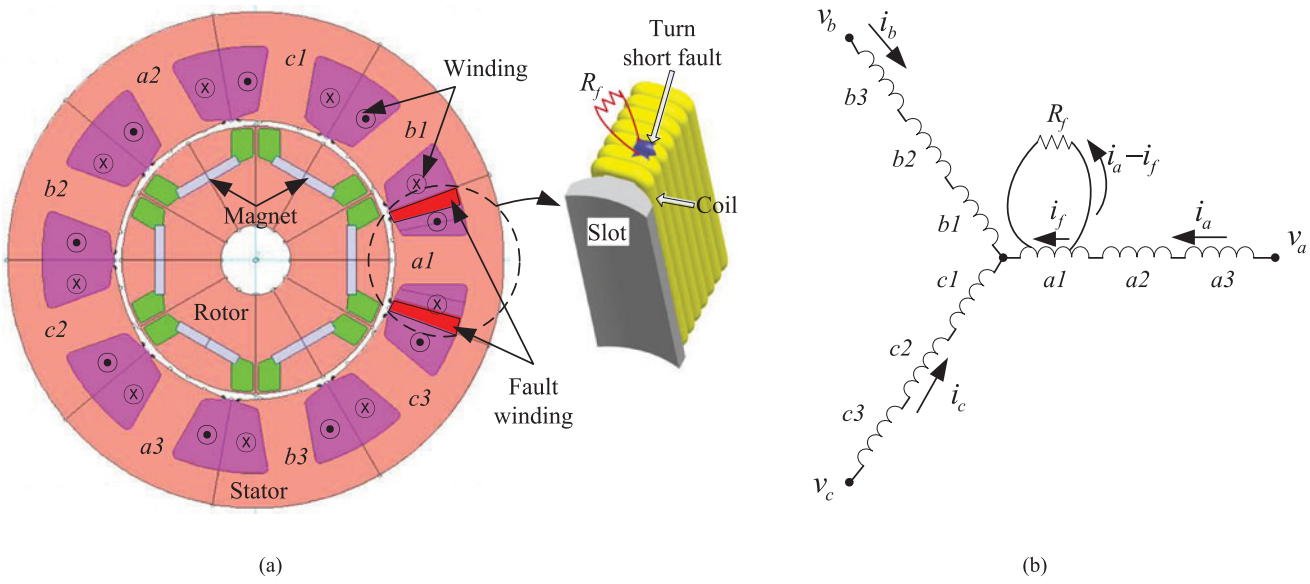

Fig. 1. (a) 6-pole-9-slot IPMSM cross-sectional figure, (b) series connected winding configuration with ITF.

$$= -\frac{2(1-x)\gamma}{P(1-\gamma)} + \frac{2x(1-x)}{P(1-\gamma)}$$

$$k_{s24} = k_{s42} = k_{s34} = k_{s43} = -\frac{1-x}{P},\ k_{s44} = \frac{2(1-x)^2}{P(1-\gamma)}.$$

R, $\omega(= d\theta/dt)$, and ψ_m denote the phase resistance, electrical angular velocity, and back-EMF constant, respectively. γ denotes the coupling factor, which was discussed by Gu *et al.* [26], to represent the coupling effect between the same windings. As the leakage inductance L_l is much less than L_1 and L_2, the leakage inductance can be assumed to be zero in (2) for simplification.

γ defines the coupled flux linkage ratio in the same phase windings. Hence, considering the flux path through the rotor structure with saliency, γ is a function of θ similar to the phase inductance. Specifically, γ has a constant value like L_1 and a sine function value like L_2. If these characteristics are considered in the IPMSM voltage equation with an ITF, this would be too complex to analyze. Here, γ is assumed to be a constant value to simplify the IPMSM voltage equation, as shown in (2).

In an inverter-fed PMSM, a negative sequence current can easily be rejected by using a negative sequence current controller, as discussed by Jeong *et al.* [24]. To simplify the model, we can therefore assume that only a positive sequence phase current without any harmonics is injected through the winding [26]

$$i_a = -I_q \sin\theta + I_d \cos\theta \tag{3}$$

$$i_b = -I_q \sin\left(\theta - \frac{2\pi}{3}\right) + I_d \cos\left(\theta - \frac{2\pi}{3}\right) \tag{4}$$

$$i_c = -I_q \sin\left(\theta + \frac{2\pi}{3}\right) + I_d \cos\left(\theta + \frac{2\pi}{3}\right). \tag{5}$$

where I_d and I_q denote the *d-q* axis currents in the SRF.

The second term on the right-hand side of (2) is the product of the inductance matrix and current matrix. As the inductance matrix has second-order harmonics, the third harmonic is produced in the flux linkage by the product of the second harmonic inductance and fundamental current. If the IPMSM has no ITF, the sum of the third harmonic flux linkage is zero. However, with an ITF, the third harmonic flux linkage is not zero and generates a third harmonic in the phase voltage and the fault current i_f. If the fault current i_f has a third harmonic, the product of the second-order inductance harmonic by the saliency and the third-order harmonic current produces the fifth harmonic flux linkage, which produces a fifth-order harmonic fault current.

$$\lambda_{abc} = \begin{bmatrix} L_l + L_1 - L_2\cos 2\theta & -\frac{L_1}{2} - L_2\cos\left(2\theta - \frac{2\pi}{3}\right) & -\frac{L_1}{2} - L_2\cos\left(2\theta + \frac{2\pi}{3}\right) \\ -\frac{L_1}{2} - L_2\cos\left(2\theta - \frac{2\pi}{3}\right) & L_l + L_1 - L_2\cos\left(2\theta + \frac{2\pi}{3}\right) & -\frac{L_1}{2} - L_2\cos 2\theta \\ -\frac{L_1}{2} - L_2\cos\left(2\theta + \frac{2\pi}{3}\right) & -\frac{L_1}{2} - L_2\cos 2\theta & L_l + L_1 - L_2\cos\left(2\theta - \frac{2\pi}{3}\right) \end{bmatrix} \begin{bmatrix} i_a \\ i_b \\ i_c \end{bmatrix} \tag{1}$$

Through this procedure, the fault current has multiple high odd-order harmonics. However, as the harmonic order increases, the magnitude decreases dramatically. The fundamental of the fault current is much greater than any other order harmonic. For simplification, the fault current was assumed to only have the fundamental current

$$\begin{aligned} i_f = \; & \alpha_{s1}\sin\theta + \alpha_{s2}\cos\theta + \alpha_{s3}\sin 3\theta + \alpha_{s4}\cos 3\theta \\ & + \alpha_{s5}\sin 5\theta + \alpha_{s6}\cos 5\theta + \cdots \approx \alpha_{s1}\sin\theta + \alpha_{s2}\cos\theta \end{aligned} \tag{6}$$

where α_{s1}, α_{s2}, α_{s3}, α_{s4}, α_{s5}, and α_{s6} denote coefficients of high-order harmonics.

By taking the fourth row of (2) and ignoring the third harmonic terms obtained from the product of the inductance and fundamental current, we can obtain the fault circuit equation

$$\begin{aligned} 0 = \; & \sin\theta \begin{pmatrix} -I_q R_{s41} + R_{s44}\alpha_{s1} - \omega I_d L_1 (k_{s41} - k_{s42}) \\ +\omega I_d L_2 \left(\frac{1}{2}k_{s41} - 2k_{s42}\right) - \omega k_{s44} L_1 \alpha_{s2} \\ +\frac{1}{2}\omega k_{s44} L_2 \alpha_{s2} - \omega\psi_m (1-x)\frac{2}{P} \end{pmatrix} \\ & + \cos\theta \begin{pmatrix} I_d R_{s41} + R_{s44}\alpha_{s2} - \omega I_q L_1 (k_{s41} - k_{s42}) \\ -\omega I_q L_2 \left(\frac{1}{2}k_{s41} - 2k_{s42}\right) + \omega k_{s44} L_1 \alpha_{s1} \\ +\frac{1}{2}\omega k_{s44} L_2 \alpha_{s1} \end{pmatrix} \end{aligned} \tag{7}$$

$\sin\theta$ and $\cos\theta$ are mutually orthogonal. To satisfy (7) for any θ, the coefficients of $\sin\theta$ and $\cos\theta$ should be zero. Hence, from (7), α_{s1} and α_{s2} can be obtained as (8) shown at the bottom of the page. where $\Delta_s = R_{s44}^2 - \omega^2 k_{s44}^2 \left(\frac{1}{4}L_2^2 - L_1^2\right)$. The first, second, and third rows of (2) can be described as (9) shown at the bottom of the next page. Assuming $L_m = L_1$, the first, second, and third terms of the right-hand side of (9) are the same as those of the SPMSM model, which was described in [26]. The last term on the right-hand side of (9) represents the saliency effect. Hence, by adding the fourth term to the positive and negative sequence voltage equations of the SPMSM model, the whole IPMSM model with an ITF can be derived. Based on (9) and [26], the positive and negative sequence voltage equations can be derived as (10) and (11) as shown at the bottom of the next page, where

$$\begin{bmatrix} v_a \\ v_b \\ v_c \end{bmatrix} = \mathbf{T}\mathbf{e}^{-\mathbf{J}\theta} \begin{bmatrix} V_{de}^+ \\ V_{qe}^+ \end{bmatrix} + \mathbf{T}\mathbf{e}^{\mathbf{J}\theta} \begin{bmatrix} V_{de}^- \\ V_{qe}^- \end{bmatrix},$$

$$\mathbf{T} = \begin{bmatrix} 1 & 0 \\ -\frac{1}{2} & \frac{\sqrt{3}}{2} \\ -\frac{1}{2} & -\frac{\sqrt{3}}{2} \end{bmatrix}, \mathbf{e}^{\mathbf{J}\theta} = \begin{bmatrix} \cos\theta & \sin\theta \\ -\sin\theta & \cos\theta \end{bmatrix}.$$

Here, $\left[V_{de}^+ V_{qe}^+\right]^T$ and $\left[V_{de}^- V_{qe}^-\right]^T$ denote the positive and negative sequence voltages, respectively. The first terms of (10) and (11) are from the SPMSM ITF model, and the second term represent the saliency obtained by transforming the last term of (9) into the positive and negative sequence SRFs.

The IPMSM torque is the sum of the magnet torque and reluctance torque. The magnet torque was described in [26]. Here, we derive the reluctance torque generated by the saliency. The reluctance torque is produced by the magnetic flux of the motor current. In terms of the magnetic flux, the total *d-q* axis motor current can be expressed as follows:

$$\begin{aligned} \begin{bmatrix} I_{de} \\ I_{qe} \end{bmatrix} &= \frac{2}{3}\mathbf{e}^{\mathbf{J}\theta}\mathbf{T}^T \begin{bmatrix} i_a - \frac{2}{P}(1-x)i_a + \frac{2}{P}(1-x)i_f \\ i_b \\ i_c \end{bmatrix} \\ &= \begin{bmatrix} \frac{4}{3P}(1-x)\cos\theta(I_q\sin\theta - I_d\cos\theta + i_f) + I_d \\ -\frac{4}{3P}(1-x)\sin\theta(I_q\sin\theta - I_d\cos\theta + i_f) + I_q \end{bmatrix} \end{aligned} \tag{12}$$

where I_{de} and I_{qe} denote the equivalent *d-q* axis current in terms of the magnetic flux vector. With the magnet torque and

$$\begin{bmatrix} \alpha_{s1} \\ \alpha_{s2} \end{bmatrix} = \frac{1}{\Delta_s} \begin{bmatrix} \begin{pmatrix} R_{s44} \begin{pmatrix} R_{s41} I_q + \omega\psi_m (1-x)\frac{2}{P} + \omega I_d L_1 (k_{s41} - k_{s42}) \\ -\omega I_d L_2 (\frac{1}{2}k_{s41} - 2k_{s42}) \end{pmatrix} \\ + \left(\omega k_{s44} L_1 - \frac{1}{2}\omega k_{s44} L_2\right) \\ \left(-R_{s41} I_d + \omega I_q L_1 (k_{s41} - k_{s42}) - \omega I_q L_2 (\frac{1}{2}k_{s41} - 2k_{s42})\right) \end{pmatrix} \\ \begin{pmatrix} R_{s44} \left(-R_{s41} I_d + \omega I_q L_1 (k_{s41} - k_{s42}) + \omega I_q L_2 (\frac{1}{2}k_{s41} - 2k_{s42})\right) \\ + \left(-\omega k_{s44} L_1 - \frac{1}{2}\omega k_{s44} L_2\right) \\ \left(-R_{s41} I_q + \omega I_d L_1 (k_{s41} - k_{s42}) - \omega I_d L_2 (\frac{1}{2}k_{s41} - 2k_{s42}) + \omega\psi_m (1-x)\frac{2}{P}\right) \end{pmatrix} \end{bmatrix} \tag{8}$$

reluctance torque, the total IPMSM torque can be derived

$$\begin{aligned}T &= \frac{3P}{4}I_q\psi_m - (1-x)\psi_m \sin\theta(-i_a+i_f) \\ &\quad -\frac{3P}{4}L_dL_qI_{de}I_{qe} \\ &= \frac{3P}{4}I_q\psi_m - (1-x)\psi_m \sin\theta(-i_a+i_f) \\ &\quad -\frac{27P}{16}(L_1^2-L_2^2)I_dI_q + \frac{9}{4}(L_1^2-L_2^2)I_d(1-x) \\ &\quad \sin\theta(-i_a+i_f) - \frac{9}{4}(L_1^2-L_2^2)I_q(1-x)\cos\theta(-i_a+i_f) \\ &\quad +\frac{3}{2P}(L_1^2-L_2^2)(1-x)^2\sin 2\theta(-i_a+i_f)^2. \end{aligned} \tag{13}$$

The first and second terms represent the magnet torque [26], and the others represent the reluctance torque generated by I_{de} and I_{qe}.

III. IPMSM Model With Parallel-Connected Winding

Fig. 2 shows a parallel-connected winding configuration with an ITF. Here, i_{p1} and i_{p2} denote the remnant healthy a1 winding current and the current of other windings, respectively. The sum of these is i_a ($i_a = i_{p1} + i_{p2}$). With three healthy windings, i_{p1} and i_{p2} are both $i_a/3$ and $2i_a/3$ and have the same current phase. However, because a turn short fault lowers the impedance in the $a1$ winding, i_{p1} and i_{p2} develop differing current magnitudes and phases. Thus, when analyzing a parallel-connected winding,

$$\begin{aligned}\begin{bmatrix} v_a \\ v_b \\ v_c \end{bmatrix} &= \begin{bmatrix} R_{s11} & 0 & 0 & R_{s14} \\ 0 & R_{s22} & 0 & 0 \\ 0 & 0 & R_{s33} & 0 \end{bmatrix} \begin{bmatrix} i_a \\ i_b \\ i_c \\ i_f \end{bmatrix} + \omega\psi \begin{bmatrix} -\left(1-(1-x)\frac{2}{P}\right)\sin\theta \\ -\sin(\theta-\frac{2\pi}{3}) \\ -\sin(\theta+\frac{2\pi}{3}) \end{bmatrix} \\ &\quad + L_1 \begin{bmatrix} k_{s11} & k_{s12} & k_{s13} & k_{s14} \\ k_{s21} & k_{s22} & k_{s23} & k_{s24} \\ k_{s31} & k_{s32} & k_{s33} & k_{s34} \end{bmatrix} \frac{d}{dt} \begin{bmatrix} i_a \\ i_b \\ i_c \\ i_f \end{bmatrix} \\ &\quad + L_2 \frac{d}{dt} \begin{bmatrix} -k_{s11}\cos 2\theta & 2k_{s12}\cos(2\theta-\frac{2\pi}{3}) & 2k_{s13}\cos(2\theta+\frac{2\pi}{3}) & -k_{s14}\cos 2\theta \\ 2k_{s21}\cos(2\theta-\frac{2\pi}{3}) & -k_{s22}\cos(2\theta+\frac{2\pi}{3}) & 2k_{s23}\cos 2\theta & 2k_{s24}\cos(2\theta-\frac{2\pi}{3}) \\ 2k_{s31}\cos(2\theta+\frac{2\pi}{3}) & 2k_{s32}\cos 2\theta & -k_{s33}\cos(2\theta-\frac{2\pi}{3}) & 2k_{34}\cos(2\theta+\frac{2\pi}{3}) \end{bmatrix} \begin{bmatrix} i_a \\ i_b \\ i_c \\ i_f \end{bmatrix} \end{aligned} \tag{9}$$

$$\begin{aligned}\begin{bmatrix} V_{de}^+ \\ V_{qe}^+ \end{bmatrix} &= \frac{1}{3} \begin{bmatrix} \begin{pmatrix} (R_{s11}+2R_{s22})I_d + R_{s14}\alpha_{s2} + \omega L_1(k_{s14}-k_{s24})\alpha_{s1} \\ +\omega L_1(-k_{s11}+2k_{s12}-2k_{s22}+k_{s23})I_q \end{pmatrix} \\ \begin{pmatrix} (R_{s11}+2R_{s22})I_q - R_{s14}\alpha_{s1} + \omega L_1(k_{s14}-k_{s24})\alpha_{s2} \\ -\omega L_1(-k_{s11}+2k_{s12}-2k_{s22}+k_{s23})I_d + (3-\frac{2}{P}(1-x))\omega\psi_m \end{pmatrix} \end{bmatrix} \\ &\quad +\frac{\omega L_2}{6} \begin{bmatrix} (-k_{s11}+8k_{s12}-2k_{s22}+4k_{s23})I_q + (k_{s14}-4k_{s24})\alpha_{s1} \\ (-k_{s11}+8k_{s21}-2k_{s22}+4k_{s23})I_d + (-k_{s14}+4k_{s24})\alpha_{s2} \end{bmatrix} \end{aligned} \tag{10}$$

$$\begin{aligned}\begin{bmatrix} V_{de}^- \\ V_{qe}^- \end{bmatrix} &= \frac{1}{3} \begin{bmatrix} \begin{pmatrix} (R_{s11}-R_{s22})I_d + R_{s14}\alpha_{s2} + \omega L_1(k_{s14}-k_{s24})\alpha_{s1} \\ +\omega L_1(-k_{s11}+2k_{s12}+k_{s22}-2k_{s23})I_q \end{pmatrix} \\ \begin{pmatrix} -(R_{s11}+2R_{s22})I_q + R_{s14}\alpha_{s1} - \omega L_1(k_{s14}-k_{s24})\alpha_{s2} \\ +\omega L_1(-k_{s11}+2k_{s12}+k_{s22}-2k_{s23})I_d + \frac{2}{P}(1-x)\omega\psi_m \end{pmatrix} \end{bmatrix} \\ &\quad +\frac{\omega L_2}{6} \begin{bmatrix} (-k_{s11}+2k_{s12}+k_{s22}-2k_{s23})I_q + (k_{s14}+2k_{s24})\alpha_{s1} \\ (k_{s11}-2k_{s21}-k_{s22}+2k_{s23})I_d + (k_{s14}+2k_{s24})\alpha_{s2} \end{bmatrix} \end{aligned} \tag{11}$$

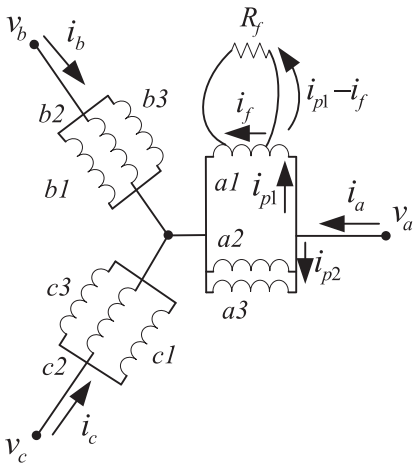

Fig. 2. Parallel-connected winding configuration with turn short fault.

not only the fault current but also the current distribution in the healthy winding must be considered [26].

As with a series connection, the voltage dynamic equation of an IPMSM with a turn short fault can be obtained with (1) and [26]

$$\begin{bmatrix} v_a \\ v_a \\ v_b \\ v_c \\ 0 \end{bmatrix} = \mathbf{R_p} \begin{bmatrix} i_{p1} \\ i_{p2} \\ i_b \\ i_c \\ i_f \end{bmatrix} + \frac{d}{dt}\mathbf{L_p} \begin{bmatrix} i_{p1} \\ i_{p2} \\ i_b \\ i_c \\ i_f \end{bmatrix} + \omega\psi_m \begin{bmatrix} -x\sin\theta \\ -\sin\theta \\ -\sin(\theta - 2\pi/3) \\ -\sin(\theta + 2\pi/3) \\ (x-1)\sin\theta \end{bmatrix} \tag{14}$$

where

$$\mathbf{R_p} = \begin{bmatrix} R_{p11} & 0 & 0 & 0 & R_{p15} \\ 0 & R_{p22} & 0 & 0 & 0 \\ 0 & 0 & R_{p33} & 0 & 0 \\ 0 & 0 & 0 & R_{p44} & 0 \\ R_{p51} & 0 & 0 & 0 & R_{p55} \end{bmatrix},$$

$$\mathbf{L_p} = \begin{bmatrix} L_{p11} & L_{p12} & L_{p13} & L_{p14} & L_{p15} \\ L_{p21} & L_{p22} & L_{p23} & L_{p24} & L_{p25} \\ L_{p31} & L_{p32} & L_{p33} & L_{p34} & L_{p35} \\ L_{p41} & L_{p42} & L_{p43} & L_{p44} & L_{p45} \\ L_{p51} & L_{p52} & L_{p53} & L_{p54} & L_{p55} \end{bmatrix}$$

$$R_{p11} = x\frac{P}{2}R + R_f, R_{p15} = R_{s51} = -R_f, R_{p22} = \frac{PR}{P-2},$$

$$R_{p33} = R_{p44} = R,$$

$$R_{s55} = (1-x)\frac{P}{2}R + R_f$$

$$L_{pij} = \begin{cases} k_{pij}(L_1 - L_2\cos 2\theta) & \text{if (i, j)} = (1,1), \\ & (1,2),(1,5),(2,1), \\ & (2,2),(2,5),(5,1), \\ & (5,2),(5,5) \\ k_{pij}\left(L_1 - L_2\cos\left(2\theta + \frac{2\pi}{3}\right)\right) & \text{if (i, j)} = (3,3) \\ k_{pij}\left(L_1 - L_2\cos\left(2\theta - \frac{2\pi}{3}\right)\right) & \text{if (i, j)} = (4,4) \\ k_{pij}(L_1 + 2L_2\cos 2\theta) & \text{if (i, j)} = (3,4), \\ & (4,3) \\ k_{pij}\left(L_1 + 2L_2\cos\left(2\theta - \frac{2\pi}{3}\right)\right) & \text{if (i, j)} = (1,3), \\ & (2,3),(3,1),(3,2), \\ & (3,5),(5,3) \\ k_{pij}\left(L_1 + 2L_2\cos\left(2\theta + \frac{2\pi}{3}\right)\right) & \text{if (i, j)} = (1,4), \\ & (2,4),(4,1),(4,2), \\ & (4,5),(5,4) \end{cases}$$

$$k_{p11} = \frac{Px^2}{2(1-\gamma)}, k_{p12} = k_{p21} = \frac{Px\gamma}{(P-2)(1-\gamma)}, k_{p13}$$
$$= k_{p31} = \frac{-x}{2}, k_{p15} = k_{p51} = \frac{Px(1-x)}{2(1-\gamma)},$$
$$k_{p22} = \frac{P}{P-2}\left(1 + \frac{2\gamma}{(1-\gamma)(P-2)}\right), k_{p23} = k_{p32} = k_{p24}$$
$$= k_{p42} = k_{p34} = k_{p43} = -\frac{1}{2},$$
$$k_{p25} = k_{p52} = \frac{P(1-x)\gamma}{(P-2)(1-\gamma)}, k_{p33} = k_{p44} = 1, k_{p35}$$
$$= k_{p53} = k_{p45} = k_{p54} = -\frac{1-x}{2}, k_{p55} = \frac{P(1-x)^2}{2(1-\gamma)}.$$

As discussed in the previous section for a series-connected winding, the same analysis can be used to develop a steady-state equation for a parallel-connected winding. The $a1$ winding current i_{p1}, remnant winding current i_{p2}, and fault current, i_f can be defined as

$$i_{p1} = \alpha_{p1}\sin\theta + \alpha_{p2}\cos\theta \tag{15}$$
$$i_{p2} = -(I_q + \alpha_{p1})\sin\theta + (I_d - \alpha_{p2})\cos\theta \tag{16}$$
$$i_f = \beta_{p1}\sin\theta + \beta_{p2}\cos\theta \tag{17}$$

where α_{p1}, α_{p2}, β_{p1}, and β_{p2} denote the coefficients of the sine and cosine function. From the first, second, and last rows of (14), detailed descriptions of α_{p1}, α_{p2}, β_{p1}, and β_{p2} are obtained

$$\begin{bmatrix} \alpha_{p1} & \alpha_{p2} & \beta_{p1} & \beta_{p2} \end{bmatrix}^T = \mathbf{A_p}^{-1}\mathbf{B_p} \tag{18}$$

where, see the unnumbered equation as shown ath the bottom the page From the second, third, and fourth rows of (14) and with (15)–(17), the phase voltage equation can be given as

$$\begin{bmatrix} v_a \\ v_b \\ v_c \end{bmatrix} = \begin{bmatrix} R_{p22} i_{p2} \\ R_{p33} i_b \\ R_{p44} i_c \end{bmatrix} + L_1 \begin{bmatrix} k_{p21} & k_{p22} & k_{p23} & k_{p24} & k_{p25} \\ k_{p31} & k_{p32} & k_{p33} & k_{p34} & k_{p35} \\ k_{p41} & k_{p42} & k_{p43} & k_{p44} & k_{p45} \end{bmatrix} \frac{d}{dt} \begin{bmatrix} i_{p1} \\ i_{p2} \\ i_b \\ i_c \\ i_f \end{bmatrix} + \omega \psi_m \begin{bmatrix} -\sin\theta \\ -\sin(\theta - 2\pi/3) \\ -\sin(\theta + 2\pi/3) \end{bmatrix}$$

$$+ L_2 \frac{d}{dt} \begin{bmatrix} -k_{p21}\cos 2\theta - k_{p22}\cos 2\theta \\ 2k_{p23}\cos\left(2\theta - \frac{2\pi}{3}\right) 2k_{p24}\cos\left(2\theta + \frac{2\pi}{3}\right) - k_{p25}\cos 2\theta \\ 2k_{p31}\cos\left(2\theta - \frac{2\pi}{3}\right) 2k_{p32}\cos\left(2\theta - \frac{2\pi}{3}\right) \\ -k_{p33}\cos\left(2\theta + \frac{2\pi}{3}\right) 2k_{p34}\cos 2\theta 2k_{p35}\cos\left(2\theta - \frac{2\pi}{3}\right) \\ 2k_{p41}\cos\left(2\theta + \frac{2\pi}{3}\right) 2k_{p42}\cos\left(2\theta + \frac{2\pi}{3}\right) \\ 2k_{p43}\cos 2\theta - k_{p44}\cos\left(2\theta - \frac{2\pi}{3}\right) 2k_{p45}\cos\left(2\theta + \frac{2\pi}{3}\right) \end{bmatrix} \begin{bmatrix} i_{p1} \\ i_{p2} \\ i_b \\ i_c \\ i_f \end{bmatrix}. \tag{19}$$

If $L_m = L_1$ like in the series-connected winding case, the first, second, and third terms of the right-hand side of the equation are the same as the SPMSM equations described in [26]. Hence, by adding the SPMSM model and the fourth term in the *d-q* rotating reference frame, the positive and negative sequence voltage equations can be derived as follows:

The second terms of (20) and (21), shown at the bottom of the next page, represent the saliency. As described in the previous section, the IPMSM torque is the sum of the magnet and reluctance torques. The reluctance torque depends on the magnetic flux produced by each total *d-q* axis current in the SRF. In terms of the magnetic flux, the total *d-q* axis motor current can be expressed as follows:

$$\begin{bmatrix} I_{de} \\ I_{qe} \end{bmatrix} = \frac{2}{3} \mathbf{e}^{\mathbf{J}\theta} \mathbf{T}^T \begin{bmatrix} i_{p2} + x i_{p1} + (1-x) i_f \\ i_b \\ i_c \end{bmatrix}$$

$$\mathbf{A_p} = \begin{bmatrix} R_{p11} + R_{p22} & \begin{pmatrix} \omega(-k_{p11} + 2k_{p12} - k_{p22}) \\ \left(L_1 - \frac{L_2}{2}\right) \end{pmatrix} & R_{p15} & \begin{pmatrix} \omega(-k_{p15} + k_{p25}) \\ \left(L_1 - \frac{L_2}{2}\right) \end{pmatrix} \\ \begin{pmatrix} \omega(k_{p11} - 2k_{p12} + k_{p22}) \\ \left(L_1 + \frac{L_2}{2}\right) \end{pmatrix} & R_{p11} + R_{p22} & \begin{pmatrix} \omega(k_{p15} - k_{p25}) \\ \left(L_1 + \frac{L_2}{2}\right) \end{pmatrix} & R_{p15} \\ R_{p51} & \begin{pmatrix} \omega(-k_{p51} + k_{p52}) \\ \left(L_1 - \frac{L_2}{2}\right) \end{pmatrix} & R_{p55} & -\omega k_{p55}\left(L_1 - \frac{L_2}{2}\right) \\ \begin{pmatrix} \omega(k_{p51} - k_{p52}) \\ \left(L_1 + \frac{L_2}{2}\right) \end{pmatrix} & R_{p51} & \omega k_{p55}\left(L_1 + \frac{L_2}{2}\right) & R_{p55} \end{bmatrix}$$

$$\mathbf{B_p} = \begin{bmatrix} \omega L_1(k_{p12} - k_{p13} - k_{p22} + k_{p23}) I_d - R_{p22} I_q + \omega \frac{L_2}{2}(-k_{p12} + 4k_{p13} + k_{p22} - 4k_{p23}) I_d + (x-1)\omega\psi_m \\ \omega L_1(k_{p12} - k_{p13} - k_{p22} + k_{p23}) I_q + R_{p22} I_d + \omega \frac{L_2}{2}(k_{p12} - 4k_{p13} - k_{p22} + 4k_{p23}) I_q \\ \omega L_1(k_{p52} - k_{p53}) I_d - \omega \frac{L_2}{2}(-k_{p52} - 4k_{p53}) I_d - (x-1)\omega\psi_m \\ \omega L_1(k_{p52} - k_{p53}) I_q - \omega \frac{L_2}{2}(k_{p52} - 4k_{p53}) I_q \end{bmatrix}$$

$$= \begin{bmatrix} \frac{2}{3}(1-x)\cos\theta(-i_{p1}+i_f)+I_d \\ -\frac{2}{3}(1-x)\sin\theta(-i_{p1}+i_f)+I_q \end{bmatrix}. \quad (22)$$

With the magnet and reluctance torques, the total IPMSM torque can be derived

$$\begin{aligned} T &= \frac{3P}{4}I_q\psi_m - (1-x)\psi_m \sin\theta(-i_a+i_f) - \frac{3P}{4}L_dL_qI_{de}I_{qe} \\ &= \frac{3P}{4}I_q\psi_m - (1-x)\psi_m \sin\theta(-i_a+i_f) - \frac{27P}{16}(L_1^2-L_2^2) \\ &\quad I_dI_q + \frac{9P}{8}(L_1^2-L_2^2)I_d(1-x)\sin\theta(-i_{p1}+i_f) \\ &\quad -\frac{9P}{8}(L_1^2-L_2^2)I_q(1-x)\cos\theta(-i_{p1}+i_f) \\ &\quad +\frac{3P}{8}(L_1^2-L_2^2)(1-x)^2\sin 2\theta(-i_{p1}+i_f)^2. \end{aligned} \quad (23)$$

The first and second terms of (22) represent the magnet torque, and the others represent the reluctance torque.

IV. FEM Simulation, Measurement, and Discussion

We performed FEM simulations to validate the ITF model with the series and parallel winding connections presented in this paper. Fig. 3 shows (a) an FEM mesh generation of the IPMSM model and external circuit models of the (b) series- and (c) parallel-connected windings. Here, i_{Rf} denotes the fault resistor current and can be defined as $i_{Rf} = i_a - i_f$ and $i_{Rf} = i_{p1} - i_f$ for the series- and parallel-connected windings, respectively. In Fig. 3(b) and (c), a1 is composed of three windings, and the turn short fault winding is connected to R_f and a switch that, when turned ON, puts the winding under a turn short fault. Three windings of $a1$ were located at the inside, middle, and outside of the slot to check the dependency of the fault winding location. However, there were small differences in the faulty winding location. All FEM simulation results were for a middle winding fault. Balanced three-phase current sources were connected to each phase winding. Table I lists the system parameters. L_1, L_2, and γ were obtained from FEM simulations [26]. Under dc current injection into a-phase windings which are $a1$, $a2$, and $a3$, L_1, L_2, and γ are given with windings flux linkage data from FEM simulation. ψ_m is also obtained from the FEM simulation with the permanent magnet data and R is calculated using the coil design data.

TABLE I
Motor Specifications

Items	Values	Units
Pole number	6	
Rated phase current	10	$[A_{\text{peak}}]$
Rated phase to phase voltage	27	$[V_{\text{rms}}]$
L_1	702	$[\mu H]$
L_2	147	$[\mu H]$
Phase resistance R	0.129	$[\Omega]$
Turn short resistance R_f of series/parallel PMSM	0.01/0.1	$[\Omega]$
Healthy turn ration x	0.5833	
Coupling factor γ	0.15135	

Figs. 4 and 5 compare the negative sequence voltage vectors in the SRF, and the fault resistor current's cosine ($I_d - \alpha_{s2}$) and sine ($I_q - \alpha_{s1}$) terms of the series-connected winding IPMSM, respectively. These were derived with the FEM simulation and proposed IPMSM ITF model. The current magnitude I_s and θ_l denotes the phase current magnitude and current load angle, respectively. They have the following relationship with the *d-q* axis current:

$$I_d = -I_s\sin\theta_l, I_q = I_s\cos\theta_l. \quad (24)$$

$$\begin{bmatrix} V_{de}^+ \\ V_{qe}^+ \end{bmatrix} = \frac{1}{3}\begin{bmatrix} \begin{pmatrix} (R_{p22}+2R_{p33})I_d + \omega L_1(-k_{p22}+2k_{p23}-2k_{p33}+k_{p34})I_q \\ +\omega L_1(k_{p21}-k_{p22}-k_{p31}+k_{p32})\alpha_{p1} - R_{p22}\alpha_{p2} + \omega L_1(k_{p25}-k_{p35})\beta_{p1} \end{pmatrix} \\ \begin{pmatrix} (R_{p22}+2R_{p33})I_q + \omega L_1\left(k_{p22}-2k_{p23}+2k_{p33}+\frac{k_{p34}}{2}\right)I_d \\ +\omega L_1(k_{p21}-k_{p22}-k_{p31}+k_{p32})\alpha_{p2} + R_{p22}\alpha_{p1} + \omega L_1(k_{p25}-k_{p35})\beta_{p2} + 3\omega\psi_m \end{pmatrix} \end{bmatrix} + \frac{\omega L_2}{6}\begin{bmatrix} (k_{p21}-k_{p22}-4k_{p31}+4k_{p32})\alpha_{p1} - (k_{p22}-16k_{p32})I_q + (k_{p25}-4k_{p35})\beta_{p1} \\ (-k_{p21}+k_{p22}+4k_{p31}-4k_{p32})\alpha_{p2} - (k_{p22}-16k_{p23})I_d - (k_{p25}-4k_{p35})\beta_{p2} \end{bmatrix} \quad (20)$$

$$\begin{bmatrix} V_{de}^- \\ V_{qe}^- \end{bmatrix} = \frac{1}{3}\begin{bmatrix} \begin{pmatrix} (R_{p22}-R_{p33})I_d + \omega L_1(-k_{p22}+2k_{p23}-2k_{p34}+k_{p33})I_q \\ +\omega L_1(k_{p21}-k_{p22}-k_{p31}+k_{p32})\alpha_{p1} - R_{p22}\alpha_{p2} + \omega L_1(k_{p25}-k_{p35})\beta_{p1} \end{pmatrix} \\ \begin{pmatrix} (-R_{p22}+R_{p33})I_q + \omega L_1\left(-k_{p22}+2k_{p23}+k_{p33}-\frac{k_{p34}}{2}\right)I_d \\ +\omega L_1(-k_{p21}+k_{p22}+k_{p31}-k_{p32})\alpha_{p2} - R_{p22}\alpha_{p1} + \omega L_1(-k_{p25}+k_{p35})\beta_{p2} \end{pmatrix} \end{bmatrix} + \frac{\omega L_2}{6}\begin{bmatrix} (k_{p21}-k_{p22}+2k_{p31}-2k_{p32})\alpha_{p1} - (k_{p22}+2k_{p32})I_q + (2k_{p35}+k_{p25})\beta_{p1} \\ (k_{p21}-k_{p22}+2k_{p31}-2k_{p32})\alpha_{p2} + (k_{p22}+2k_{p32})I_d + (2k_{p35}+k_{p25})\beta_{p2} \end{bmatrix} \quad (21)$$

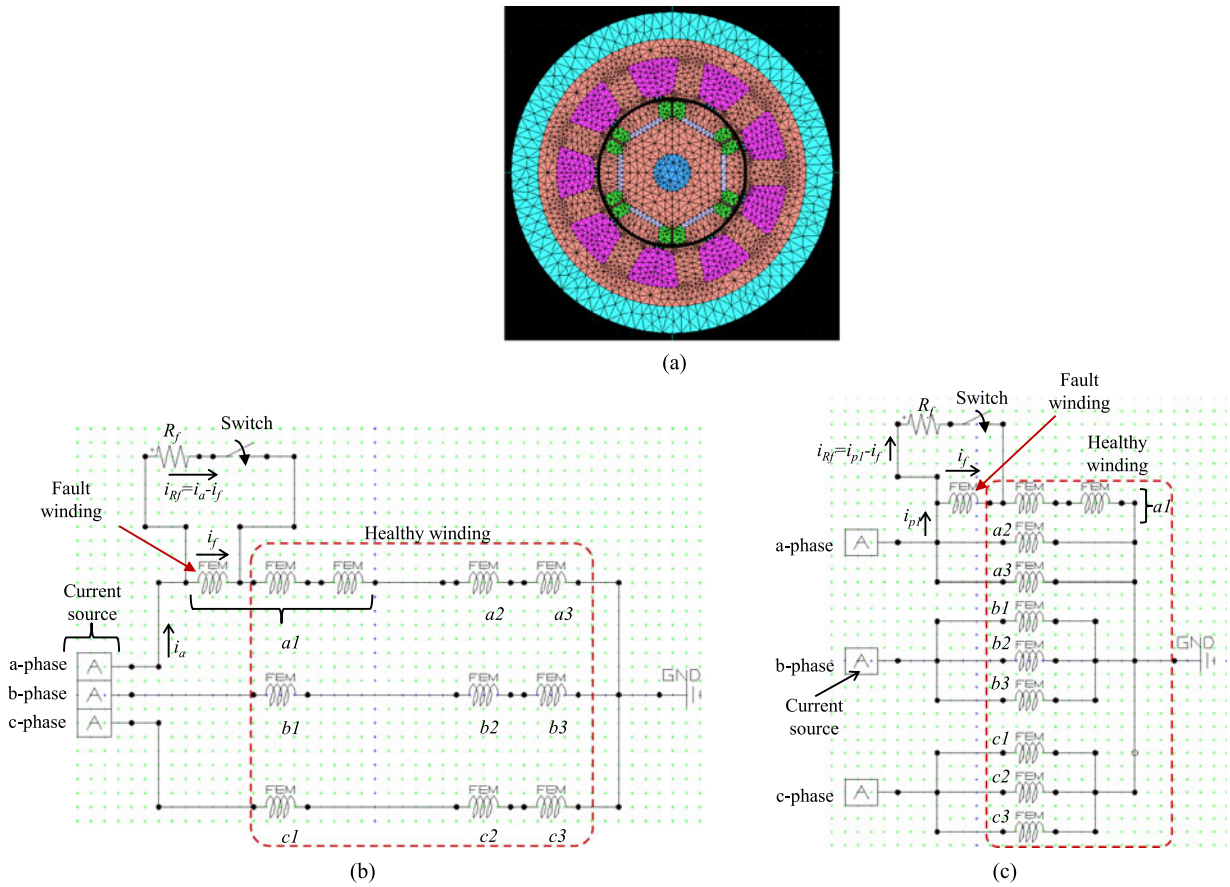

Fig. 3. FEM simulation models: (a) IPMSM mesh model, (b) FEM circuit model of series-connected windings, and (c) FEM circuit model of parallel-connected windings.

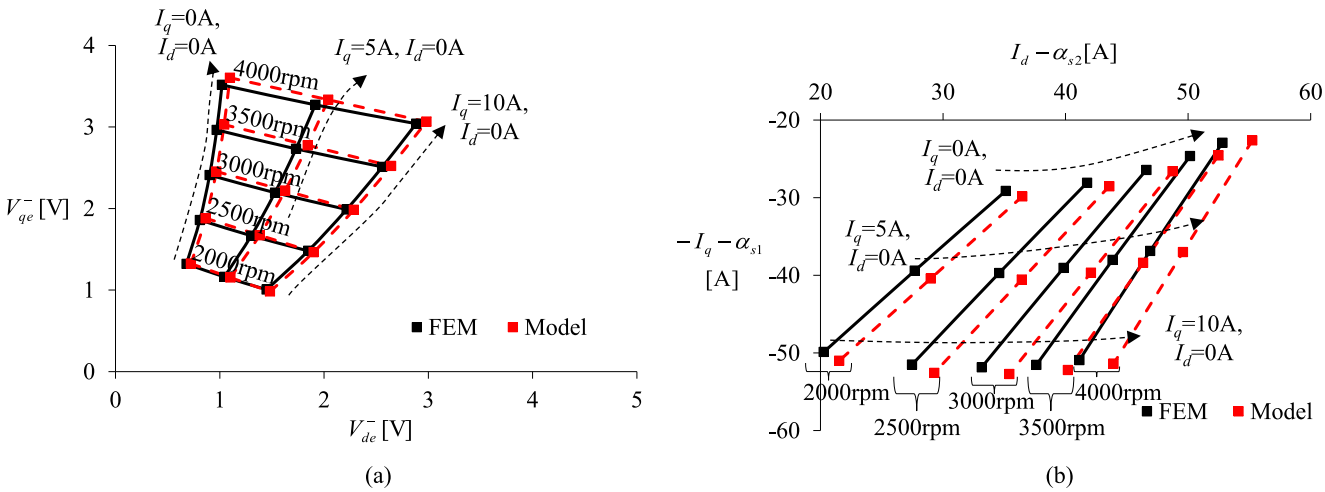

Fig. 4. Series winding connection IPMSM: (a) negative sequence voltage, (b) cosine and sine term magnitudes of fault resistor current $i_{rf}(= i_a - i_f)$ for various speeds and $\theta_l = 0$ using FEM simulation and proposed model for turn short fault in a-phase winding.

Fig. 4 graphs when θ_l was fixed to zero and the speed was varied from 2000 to 4000 r/min. In contrast, Fig. 5 graphs when the speed was fixed to 3500 r/min and θ_l was varied from zero to $\pi/3$. As the speed of the rotation increased, the negative sequence voltage in the SRF increased. As the phase current increased, the negative sequence voltage vector rotated anti-clockwise when θ_l was zero (see Fig. 4). However, when θ_l was large, the negative I_d increases by (23). As a negative I_d decreased the total air-gap flux, the negative sequence voltage and fault resistor current decreased as θ_l increased. The results of the proposed model were almost identical to the FEM simulation results.

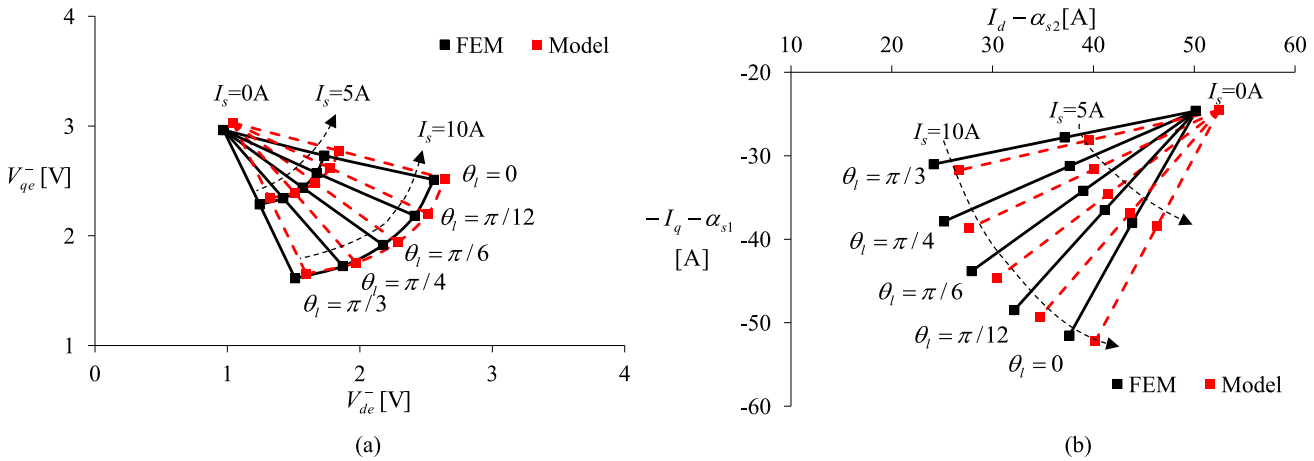

Fig. 5. Series winding connection IPMSM: (a) negative sequence voltage, (b) cosine and sine term magnitudes of fault resistor current $i_{rf}(= i_a - i_f)$ at 3500 r/min and $\theta_l = 0, \pi/12, \pi/6, \pi/4, \pi/3$ using FEM simulation and proposed model for turn short fault in a-phase winding.

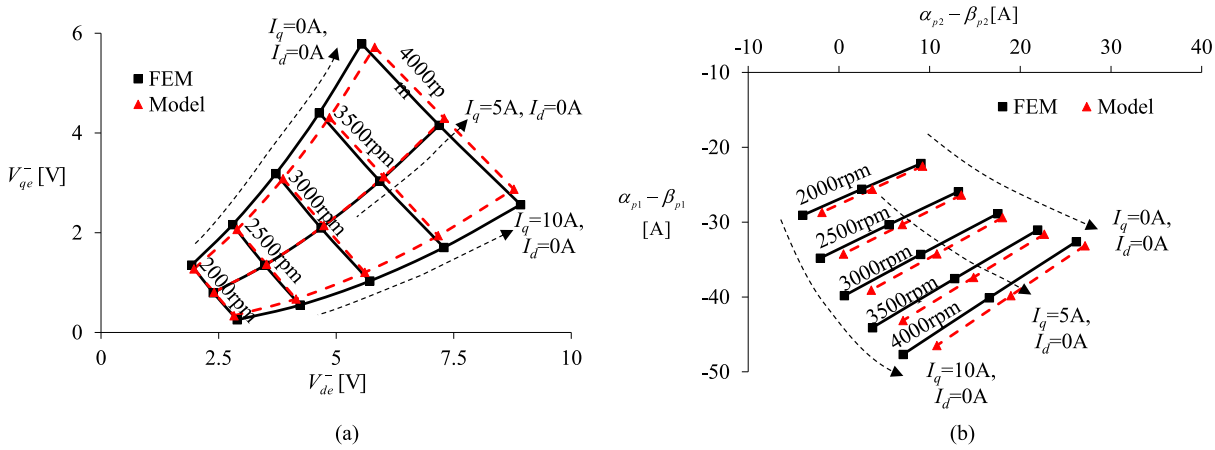

Fig. 6. Parallel winding connection PMSM: (a) negative sequence voltage, (b) cosine and sine term magnitudes of fault resistor current $i_{rf}(= i_{p1} - i_f)$ for various speeds and $\theta_l = 0$ using FEM simulation and proposed model for turn short fault in a-phase winding.

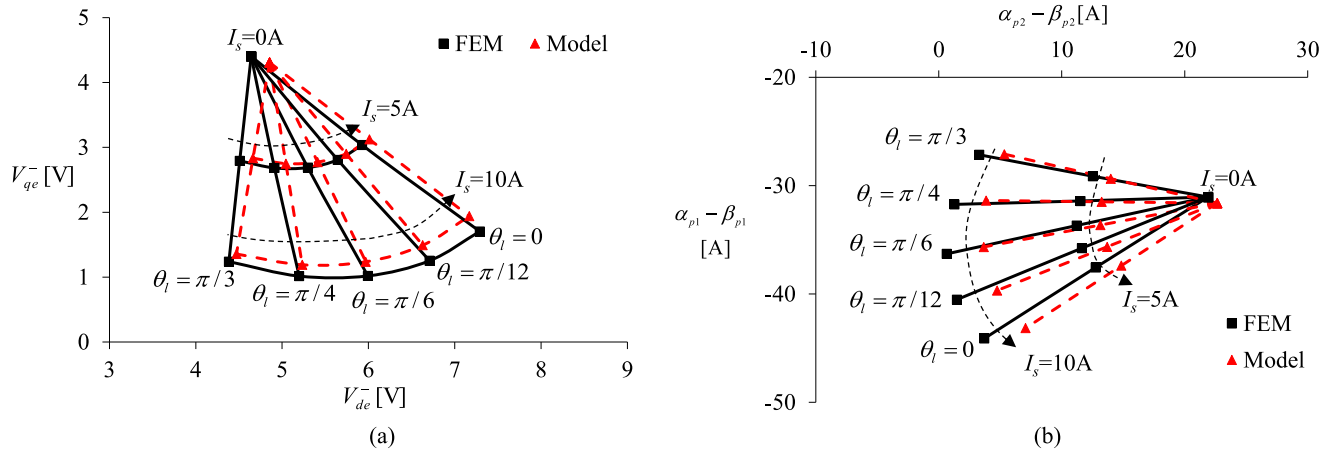

Fig. 7. Parallel winding connection PMSM: (a) negative sequence voltage, (b) cosine and sine term magnitudes of fault resistor current $i_{rf}(= i_{p1} - i_f)$ at 3500 r/min and $\theta_l = 0, \pi/12, \pi/6, \pi/4, \pi/3$ using FEM simulation and proposed model for turn short fault in a-phase winding.

TABLE II
DIFFERENCE BETWEEN FEM SIMULATION AND PROPOSED IPMSM ITF MODEL (FIGS. 4–7)

Speed [r/min]	I_q [A]	Difference [%]							
		Series winding (Fig. 4)				Parallel winding (Fig. 6)			
		$\varepsilon(\mathbf{V}^-_{\mathbf{dqe}})$	$\varepsilon(\lvert\mathbf{V}^-_{\mathbf{dqe}}\rvert)$	$(\varepsilon\mathbf{I}_{\mathbf{Rf}})$	$\varepsilon(\lvert\mathbf{I}_{\mathbf{Rf}}\rvert)$	$(\varepsilon\mathbf{V}^-_{\mathbf{dqe}})$	$(\varepsilon\lvert\mathbf{V}^-_{\mathbf{dqe}}\rvert)$	$(\varepsilon\mathbf{I}_{\mathbf{Rf}})$	$(\varepsilon\lvert\mathbf{I}_{\mathbf{Rf}}\rvert)$
	0	2.9	1.5	3.3	3.3	3.8	0.0	1.6	1.6
2000	5	3.7	2.1	3.4	3.3	0.7	0.7	4.5	0.6
	10	2.3	0.7	3.1	2.8	3.7	2.0	7.3	2.1
	0	3.0	2.1	3.7	3.5	3.8	0.6	1.9	1.9
2500	5	3.8	2.6	3.9	3.5	1.1	1.1	4.8	0.9
	10	2.3	1.3	3.6	3.1	3.5	1.6	7.5	1.8
	0	3.0	2.5	4.0	3.6	3.7	1.0	2.2	2.1
3000	5	3.7	2.9	4.1	3.6	1.5	1.5	5.0	1.2
	10	2.3	1.6	3.9	3.2	3.5	1.2	7.7	1.5
	0	3.1	2.7	4.1	3.7	3.6	1.5	2.4	2.3
3500	5	3.7	3	4.3	3.7	1.8	1.7	5.3	1.4
	10	2.4	1.9	4.2	3.3	3.6	0.8	7.9	1.2
	0	3.1	2.9	4.3	3.7	3.5	1.8	2.6	2.5
4000	5	3.6	3.1	4.5	3.7	2.1	2.0	5.5	1.6
	10	2.4	2	4.3	3.3	3.7	0.5	8.1	1.0
θ [deg.]	I_q [A]	Difference [%]							
		Series winding (Fig. 5)				Parallel winding (Fig. 7)			
		$(\mathbf{V}^-_{\mathbf{dqe}})$	$(\lvert\mathbf{V}^-_{\mathbf{dqe}}\rvert)$	$(\mathbf{I}_{\mathbf{Rf}})$	$(\lvert\mathbf{I}_{\mathbf{Rf}}\rvert)$	$(\mathbf{V}^-_{\mathbf{dqe}})$	$(\lvert\mathbf{V}^-_{\mathbf{dqe}}\rvert)$	$(\mathbf{I}_{\mathbf{Rf}})$	$(\lvert\mathbf{I}_{\mathbf{Rf}}\rvert)$
	0	3.1	2.7	4.1	3.7	3.6	1.5	2.4	2.3
60	5	3.6	3.3	5.2	4.6	3.0	2.9	4.6	2.5
	10	4.2	3.9	6.6	5.4	3.2	2.6	7.5	1.0
	0	3.1	2.7	4.1	3.7	3.6	1.5	2.4	2.3
45	5	3.6	3.2	5.1	4.4	2.7	2.7	5.2	2.1
	10	4.1	3.7	5.8	4.6	3.4	1.3	8.2	0.5
	0	3.1	2.7	4.1	3.7	3.6	1.5	2.4	2.3
30	5	3.7	3.1	4.8	4.1	2.4	2.4	5.4	1.7
	10	3.9	3.4	5.2	4.1	3.6	0.3	8.5	1.2
	0	3.1	2.7	4.1	3.7	3.6	1.5	2.4	2.3
15	5	3.7	3.1	4.6	3.9	2.1	2.0	5.5	1.5
	10	3.2	2.7	4.6	3.6	3.7	0.4	8.3	1.4
	0	3.1	2.7	4.1	3.7	3.6	1.5	2.4	2.3
0	5	3.7	3	4.3	3.7	1.8	1.7	5.3	1.4
	10	2.4	1.9	4.2	3.3	3.6	0.8	7.9	1.2

Figs. 6 and 7 compare the negative sequence voltage vector in the SRF and the fault resistor current's cosine ($\alpha_{p2} - \beta_{p2}$) and sine ($\alpha_{p1} - \beta_{p1}$) terms of the parallel winding IPMSM, respectively. These were derived using the FEM simulation and proposed IPMSM ITF model. θ_l is fixed to zero in Fig. 6, and the speed is fixed to 3500 r/min in Fig. 7. The model results were very close to the FEM results.

Table II lists the differences between the FEM simulation and proposed IPMSM ITF model of Figs. 4–7, where $\varepsilon(\cdot p)$ denotes the difference function and $\mathbf{V}^-_{\mathbf{dqe}}$ and $\mathbf{I}_{\mathbf{Rf}}$ are the negative sequence voltage and the fault resistor current in the complex domain, respectively. These are defined as follows:

$$\varepsilon(\mathbf{Z}) = \left| \frac{\{\mathbf{Z}\}_{\mathbf{FEM}} - \{\hat{\mathbf{Z}}\}_{\mathbf{model}}}{\{\mathbf{Z}\}_{\mathbf{FEM}}} \right| \times 100[\%] \tag{25}$$

$$\mathbf{V}^-_{\mathbf{dqe}} = V^-_{de} + jV^-_{qe} \tag{26}$$

$$\mathbf{I}_{\mathbf{Rf}} = \begin{cases} I_d - \alpha_{s2} - j\,(I_q + \alpha_{s1}) & : \text{series winding IPMSM} \\ \alpha_{p2} - \beta_{p2} + j\,(\alpha_{p1} - \beta_{p1}) & : \text{parallel winding IPMSM} \end{cases} \tag{27}$$

$\{\varepsilon(\mathbf{V}^-_{\mathbf{dqe}}), \varepsilon(\mathbf{I}_{\mathbf{Rf}})\}$ and $\{\varepsilon(\lvert\mathbf{V}^-_{\mathbf{dqe}}\rvert), \varepsilon(\lvert\mathbf{I}_{\mathbf{Rf}}\rvert)\}$ are the differences in the complex domain and the absolute value. For the series winding IPMSM, the difference is below 5% in most cases; therefore, the accuracy of the ITF model is excellent. It is notable, however, that the accuracy is worse for the parallel winding IPMSM at high phase currents. This is because, for the parallel winding IPMSM, the dynamics of i_{p1} as well as i_f need to be modeled.

To verify the proposed model, IPMSMs having intermediate taps for an ITF test were used. Fig. 8(a) shows a picture of series and parallel winding IPMSMs. At the back of the IPMSMs, the ITF terminal block is connected to the stator intermediate windings. Fig. 8(b) and (c) shows the three-phase terminal voltages v_a, v_b, v_c and the fault resistor current i_{Rf} of the series winding and parallel winding, respectively, at 3500 r/min, $x = 0.5833$ and $I_s = 0$. Here, no external current or voltage source was used to eliminate additional distortions. The measured phase voltage and fault resistor current were less than $I_s = 0$.

Figs. 9 and 10 plot the three-phase voltage and fault resistor current according to the measurements, FEM simulation, and proposed model. The proposed model results were almost identical to those of the FEM simulation and measured plots

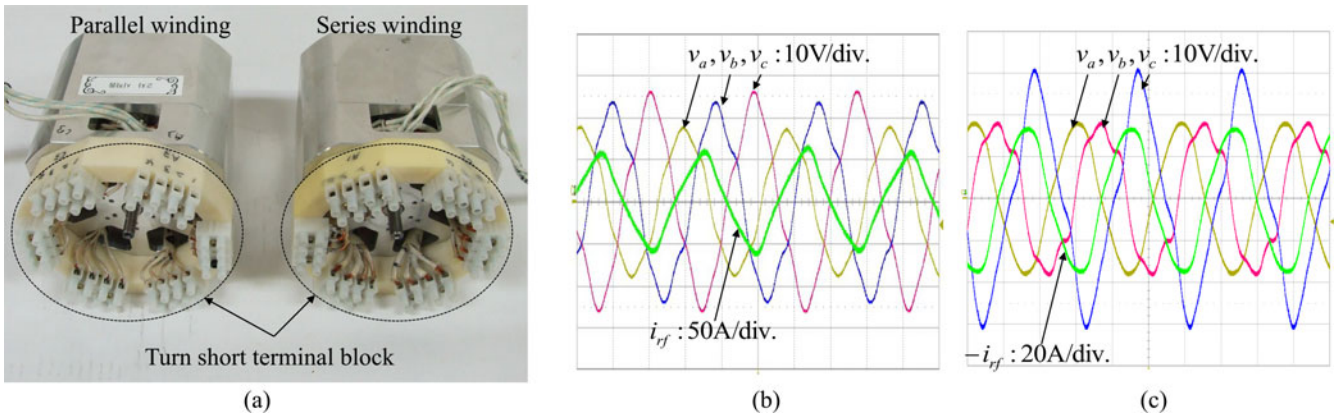

Fig. 8. (a) Picture of series and parallel winding IPMSMs with turn short fault terminal block, (b) three-phase voltage and fault current measurement results with series winding at 3500 r/min, $R_f = 0.01$ and $x = 0.5833$ (c) three-phase voltage and fault current measurement result with parallel winding at 3500 r/min, $Rf = 0.13$ and $x = 0.5833$.

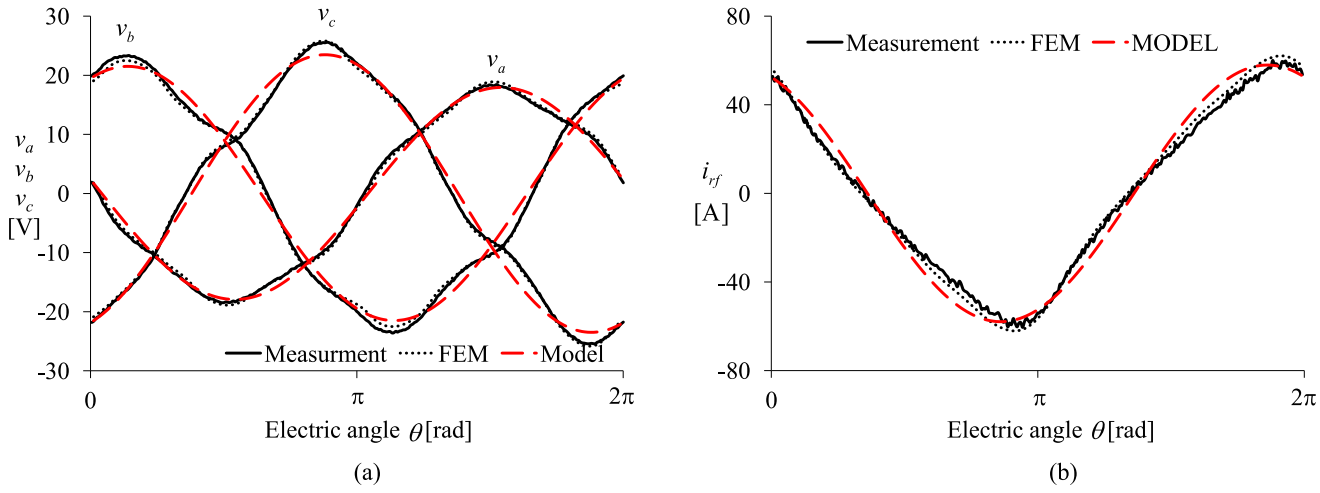

Fig. 9. Series winding connection IPMSM: (a) three-phase terminal voltage and (b) fault resistor current i_{rf} at 3500 r/min, $R_f = 0.01$ and $x = 0.5833$ according to measurement, FEM simulation, and proposed model for turn short fault in a-phase winding.

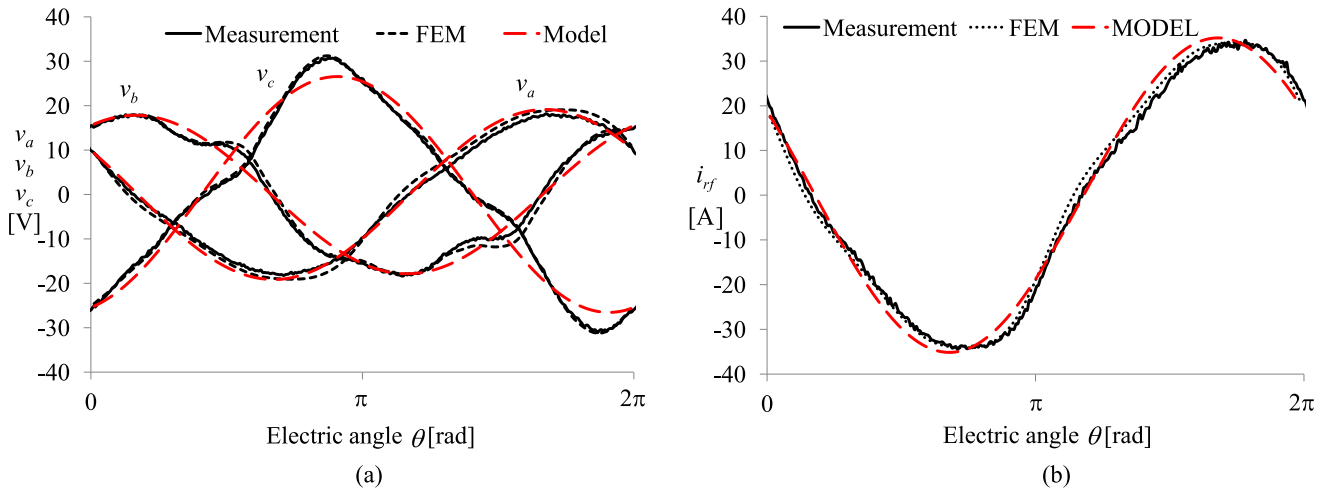

Fig. 10. Parallel winding connection IPMSM: (a) three-phase terminal voltage and (b) fault resistor current i_{rf} at 3500 r/min, $R_f = 0.13$ and $x = 0.5833$ according to measurement, FEM simulation, and proposed model for turn short fault in a-phase winding.

at the fundamental frequency. The proposed model did not include high-order harmonics modeling, which caused the difference between the proposed models plots and those of the others.

V. Concluding Remarks

In this study, ITF models of IPMSMs employing series and parallel winding connections were developed through the addition of saliency modeling to SPMSM models studied previously. The saliency effects were modeled with the deformed flux models considering cross-flux linkages. The developed models were verified by performing FEM-based simulation and measuring the back EMFs and fault resistor currents of the series and parallel IPMSMs with an ITF.

References

[1] G. Wang, H. Zhan, G. Zhang, X. Gui, and D. Xu, "Adaptive compensation method of position estimation harmonic error for EMF-based observer in sensorless IPMSM drives," *IEEE Trans. Power Electron.*, vol. 29, no. 6, pp. 3055–3064, Jun. 2014.

[2] T. D. Do, S. Kwak, H. H. Choi, and J. W. Jung, "Suboptimal control scheme design for interior permanent-magnet synchronous motors: an SDRE-based approach," *IEEE Trans. Power Electron.*, vol. 29, no. 6, pp. 3020–3031, Jun. 2014.

[3] S. Y. Jung, J. Hong, and K. Nam, "Current minimizing torque control of the IPMSM using Ferrari's method," *IEEE Trans. Power Electron.*, vol. 28, no. 12, pp. 5603–5617, Dec. 2013.

[4] P. O'Donnel, "Report of large motor reliability survey of industrial and commercial installations: Part 1," *IEEE Trans. Ind. Appl.*, vol. IA-21, no. 4, pp. 853–864, Jul./Aug. 1985.

[5] P. O'Donnel,, "Report of large motor reliability survey of industrial and commercial installations: Part 2," *IEEE Trans. Ind. Appl.*, vol. IA-21, no. 4, pp. 865–872, Jul./Aug. 1985.

[6] O. V. Thorsen and M. Dalva, "A survey of faults on induction motors in offshore oil industry, petrochemical industry, gas terminals, and oil refineries," *IEEE Trans. Ind. Appl.*, vol. 31, no. 5, pp. 1186–1196, Sep./Oct. 1995.

[7] A. H. Bonnett and G. C. Soukup, "Cause and analysis of stator and rotor failures in three-phase squirrel-cage induction motors," *IEEE Trans. Ind. Appl.*, vol. 28, no. 4, pp. 921–937, Jul./Aug. 1992.

[8] A. Gandhi, T. Corrigan, and L. Parsa, "Recent advances in modeling and online detection of stator interturn faults in electrical motors," *IEEE Trans. Ind. Electron.*, vol. 58, no. 5, 1564–1575, May 2011.

[9] M. Arkan, D. L. Perovic. and P. Unswoth, "On-line stator winding fault diagnosis in induction motors," *IEEE Proc. Electr. Power Appl.*, vol. 148, no. 6, pp. 537–547, Nov. 2001.

[10] F. Briz, M. W. Degner, A. Zamarron, and J. M. Guerrero, "On-line stator winding fault diagnosis in inverter-fed AC machines using high frequency signal injection," in *Proc. IEEE 37th Conf. Ind. Appl. IAS Annu. Meet.*, 2002, vol. 3, pp. 2094–2101.

[11] M. A. Cash, T. G. Habetler, and G. B. Kliman, "Insulation failure prediction in AC machines using line-neutral voltages," *IEEE Trans. Ind. Appl.*, vol. 34, no. 6, pp. 1234–1239, Nov./Dec. 1998.

[12] R. M. Tallam, T. G. Habetler, and R. G. Harley, "Stator winding turn-fault detection for closed-loop induction motor drives," *IEEE Trans. Ind. Appl.*, vol. 39, no. 3, pp. 720–724, May/Jun. 2003.

[13] M. A. Awadallah, M. M. Morcos, S. Gopalakrishnan, and T. W. Nehl, "A neuro-fuzzy approach to automatic diagnosis and location of stator interturn fault in CSI-Fed PM brushless DC motors," *IEEE Trans. Energy Convers.*, vol. 20, no. 2, pp. 253–259, Jun. 2005.

[14] K. H. Kim, B. G. Gu, and I. S. Jung, "Online fault-detecting scheme of an inverter-fed permanent magnet synchronous motor under stator winding shorted turn and inverter switch open," *IET Elect. Power Appl.*, vol. 5, no. 6, pp. 529–539, Jul. 2010.

[15] A. Starou, H. G. Sedding, and J. Penman, "Current monitoring for detecting inter-turn short circuits in induction motors," *IEEE Trans. Energy Convers.*, vol. 16, no. 1, pp. 32–37, Mar. 2001.

[16] B. M. Ebrahimi, and J. Faiz, "Feature extraction for short-circuit fault detection in permanent-magnet synchronous motors using stator-current monitoring," *IEEE Trans. Power Electron.*, vol. 25, no. 10, pp. 2673–2682, Oct. 2010.

[17] T. Kim, H. W. Lee, and S. Kwak, "The internal fault analysis of brushless DC motors based on the winding function theory," *IEEE Trans. Magn.*, vol. 45, no. 5, pp. 2090–2096, May 2009.

[18] K. H. Kim, D. U. Choi, B. G. Gu, and I. S. Jung, "Fault model and performance evaluation of an inverter-fed permanent magnet synchronous motor under winding shorted turn and inverter switch open," *IET Electr. Power Appl.*, vol. 4, no. 4, pp. 214–225, Apr. 2010.

[19] M. Hadef, A. Djerdir, M. R. Mekideche, and A-O. N'Diaye, "Diagnosis of stator winding short circuit faults in a direct torque controlled interior permanent magnet synchronous motor," presented at the IEEE Vehicle Power Propulsion Conf., Chicago, IL, USA, 2011.

[20] B. Vaseghi, B. Nahid-Mobarakh, N. Takorabet, and F. Meibody-Tabar, "Inductance identification and study of PM motor with winding turn short circuit fault," *IEEE Trans. Magn.*, vol. 47, no. 5, pp. 978–981, May. 2011.

[21] L. Romeral, J. Urresty, J. R. Ruiz, and A. Espinosa, "Modeling of surface-mounted permanent magnet synchronous motors with stator winding interturn faults," *IEEE Trans. Ind. Electron.*, vol. 58, no. 5, 1576–1585, May 2011.

[22] K. T. Kim, J. K. Park, B. W. Kim, and J. Hur, "Comparison of the fault characteristics of IPM-type and SPM-type BLDC motors under inter-turn faults conditions using winding function theory," in *Proc. Conf. IEEE ECCE*, 2012, pp. 12671–1269.

[23] R. Islam, M. Islam, J. Tersigni, and T. Sebstian, "Inter winding short circuit faults in permanent magnet synchronous motors used for high performance applications," in *Proc. IEEE Energy Convers. Congr. Expo.*, 2012, pp. 1291–1298.

[24] I. Jeong, B. J. Hyon, and K. Nam, "Dynamic modeling and control for SPMSMs with internal turn short faults," *IEEE Trans. Power Electron.*, vol. 28, no. 7, pp. 3495–3508, Jul. 2013.

[25] B. G. Gu, J. H. Choi, and I. S. Jung, "A dynamic modeling and a fault detection scheme of a PMSM under an inter turn short," in *Proc. IEEE Vehicle Power Propulsion Conf.*, 2012, pp. 1074–1080.

[26] B. G. Gu, J. H. Choi, and I. S. Jung, "Development and analysis of inter-turn short fault model of PMSMs with series and parallel winding connections," *IEEE Trans. Power Electron.*, vol. 29, no. 4, pp. 2016–2026, Apr. 2014.

[27] Y. S. Lee, K. T. Kim, and J. Hur, "Finite-element analysis of the demagnetization of IPM-type BLDC motor with stator turn fault," *IEEE Trans. Magn.*, vol. 50, no. 2, art. no. 7022004, Feb. 2014.

Bon-Gwan Gu received the B.S. degree from the Kyungpook National University, Daegu, Korea, in 1998, and the M.S. and Ph.D. degrees from the Pohang University of Science and Technology, Pohang, Korea, in 2000 and 2005, respectively, all in electrical engineering.

From 2005 to 2007, he was with LG electronics, Seoul, Korea. From 2008 to 2014, he was a Managerial Researcher with Korea Electronics Technology Institute, Bucheon, Korea. In 2014, he was with the Kyungpook National University as an Assistant Professor in the School of Energy Engineering. His research interests include ac motor control, dc–dc converters, and PWM converter/inverter system.